Jinlin Lu, Shihan Li, Zhiguo Luo\*, Zongshu Zou and Lei Shao

# Numerical simulation of collision removal of inclusion in swirling flow tundish

https://doi.org/10.1515/ijcre-2021-0300 Received December 27, 2021; accepted May 2, 2022; published online May 30, 2022

Abstract: The SFT (swirling flow tundish) is a kind of tundish with SC (swirl chamber) placed in the flow injection zone. The gravity potential energy of the molten steel is converted into rotation kinetic energy as entering into the tundish from the bottom of the SC along the tangential direction. The inclusions tend to collide and aggregate as following the rotating molten steel in the SC. In this work, the collision-coalescence behavior of inclusion was investigated by the mathematical simulation with PBM (population balance model) model, and the removal rate of the inclusion was investigated by the DPM model. The results show that, under the same operating conditions, the average diameter of inclusion at the outlet of the tundish increases from 4.25 µm to 4.35 µm with the introduction of the SC, which means that the SC promotes the collision and aggregation of inclusion. The inclusion removal rate of SFT is 33.09% without considering the collision-coalescence, and it increases into 43.20% as considering the collisioncoalescence. The results of considering the collisioncoalescence of inclusion is more consistent with the actual movement of inclusion in the tundish.

**Keywords:** collision-coalescence; inclusion removal; numerical simulation; swirling flow tundish.

# 1 Introduction

In the continuous casting process, the tundish mainly plays the role of storing and distributing molten steel. In recent years, to improve the quality of steel, the tundish has been developed into a continuous reactor for removing

\*Corresponding author: Zhiguo Luo, Key Laboratory for Ecological of Multimetallic Mineral of Ministry of Ministry of Education, Northeastern University, Shenyang, Liaoning, 110819, China, E-mail: luozg@smm.neu.edu.cn

Jinlin Lu, Shihan Li, Zongshu Zou and Lei Shao, Key Laboratory for Ecological of Multimetallic Mineral of Ministry of Ministry of Education, Northeastern University, Shenyang, Liaoning, 110819, China. https://orcid.org/0000-0002-0245-5485 (J. Lu)

inclusions. Therefore, more metallurgical operations can be carried out in the tundish, such as introducing weirs and dams, gas curtain technology and turbulence inhibitors, etc. These devices can improve the flow field and increase the residence time of molten steel, which is beneficial to the removal of inclusion (Chen, Xie, and Long 2014; Morales et al. 2001). However, Lopez et al. (López-Ramirez et al. 2001) found that the small inclusions are difficult to remove by floating.

The centrifugal flow tundish is a new type of tundish developed to further improve the cleanliness of molten steel (Wang, Li, and Tsukihashi 2007; Wang, Zhang, and Seetharaman 2016). The molten steel is drove to rotate by the rotating magnetic field. Due to the swirling flow, the inclusions move towards the center of the SC, which promotes the growth of inclusion due to collision-coalescence. The small inclusions collide and aggregate into large inclusions, and the large inclusions rise to the surface being absorbed by the slag. The centrifugal flow tundish requires an external magnetic field to rotate the molten steel, which means the increase of the production cost of steel. Zou et al. (Yue, Hou, and Zou 2009a) proposed a simple structure of the SFT to remove inclusions by combining the centrifugal principle of centrifugal flow tundish with the turbulence controller. The SC is introduced into the conventional tundish, and the molten steel enters into the SC along the sidewall of the SC due to the potential energy. The SC leds to the swirling flow, which achieves the same function as the centrifugal flow tundish and reduces the cost of external energy. Yue et al. (Hou and Zou 2005; Hou, Yue, and Wang 2008; Yue, Hou, and Zou 2009b; Yue, Hou, and Zou 2010) simulated the removal rate of inclusion in the SFT through water model experiments and numerical methods, but the collision-coalescence of inclusion was ignored. In actual production, the collision-coalescence of inclusion is very important. The small-size inclusions collide and aggregate into larger-size ones, which is more conducive to the removal of inclusion. Yang, Lei, and Bi (2018) investigated the spatial distribution and size of the inclusion by mass conservation model and energy conservation model. The numerical results of inclusion showed that the size distribution agreed with the experimental, but the removal rate of inclusion was ignored.

In the present work, the movement behavior of inclusion in molten steel was simulated by the PBM model and

DPM model with the help of ANSYS Fluent considering the collision-coalescence between inclusions. The collisioncoalescence of the inclusion is simulated by the PBM model, including the diameter and the quantity density of inclusion. The removal rate of inclusion is studied by the DPM model. Finally, the total removal rate of inclusion is determined by the ratio of the total volume of inclusion removed due to floating in molten steel to the initial total volume of the inclusion.

# 2 Mathematical model

### 2.1 Control equations

#### 2.1.1 Collision-coalescence model

The molten steel phase and the inclusion phase are regarded as continuous mediums. The continuity and momentum conservation equations are shown in Eqs. (1) and (2).

$$\frac{(\partial \rho_k \alpha_k)}{\partial t} + \nabla \cdot \left( \rho_k \alpha_k u_k \right) = 0 \tag{1}$$

$$\frac{\left(\partial \rho_{k} \alpha_{k} u_{k}\right)}{\partial t} + \nabla \cdot \left(\rho_{k} \alpha_{k} u_{k} u_{k}\right)$$

$$= -\alpha_{k} \nabla p + \nabla \cdot \left[\alpha_{k} \mu_{\text{eff}} \left(\nabla u_{k} + \left(\nabla u_{k}\right)^{T}\right)\right]$$

$$+ \rho_{k} \alpha_{k} g + F_{k}$$
(2)

The inclusion phase is grouped into *i*, the *i*th number density population balance equation and continuity equation are shown in Eqs. (3) and (4).

$$\frac{\partial n_i}{\partial t} + \frac{\partial}{\partial x_i} \left( u_i n_i \right) = B_a - D_a \tag{3}$$

$$\frac{\partial \left(\alpha_{p} \rho_{p} f_{i}\right)}{\partial t} + \nabla \left(\alpha_{p} \rho_{p} u_{i} f_{i}\right) = S_{i} \tag{4}$$

In the formula,  $B_a$  and  $D_a$  are the number density of the ith group inclusion due to birth and death of aggregation.  $S_i$ is the source term.  $\alpha_{\rm p}$  is the volume fraction of inclusion.  $\rho_{\rm p}$ is the density of inclusion.

$$n_i V_i = f_i \alpha_{\rm p} \tag{5}$$

$$f_i = \frac{\alpha_i}{\alpha_{\rm D}} \tag{6}$$

In the formula,  $n_i$  is the quantity density of the *i*th group;  $f_i$  is the proportion of the *i*th group to the total volume fraction of inclusion;  $\alpha_i$  is the volume fraction of the *i*th group of inclusion;  $V_i$  is the volume of one inclusion in the ith group.

When the size of the inclusion is smaller than the critical Kolmogorov of the turbulent vortex, the inertia of the inclusion is ignored and the movement of the inclusion mainly depends on the action of the viscous force. When the size of the inclusion is larger than the critical Kolmogorov, the viscous force of the inclusion is ignored and the movement of the inclusion depends on the inertial force (Kusters, Wijers, and Dirk Thoenes 1997). The Kolmogorov  $\eta$  of the *i*th group of inclusion is shown in Eq. (7)

$$\eta = \left(\frac{v^3}{\epsilon}\right)^{1/4} \tag{7}$$

In the formula,  $\nu$  is the kinematic viscosity.  $\varepsilon$  is the dissipation rate of turbulent kinetic energy.

When the size of the inclusion is smaller than the critical Kolmogorov, Saffman and Turner (1956) proposed the collision rate shown in Eq. (8)

$$\beta_{\rm T}(r_i, r_j) = \alpha \sqrt{\frac{8\pi}{15}} \frac{(d_i + d_j)^3}{8} \sqrt{\frac{\epsilon}{\nu}}$$
 (8)

In the formula,  $r_i$  and  $r_j$  are inclusions of group i and j,  $d_i$  and  $d_i$  are the diameters of group i and j.

When the size of the inclusion is larger than the critical Kolmogorov, The collision rate proposed by Abrahamson (1975) is shown in Eq. (9)

$$\beta_{\rm T}(r_i, r_j) = 2^{\frac{3}{2}} \alpha \sqrt{\pi} \frac{(d_i + d_j)^3}{4} \sqrt{U_i^2 + U_j^2}$$
 (9)

In the formula,  $U_i$  and  $U_j$  are the velocity of inclusion in groups i and j.

#### 2.1.2 Movement model of inclusion

The movement of inclusion is calculated by the Lagrangian method according to the force balance, the calculation method of the inclusion is shown in Eq. (10).

$$\frac{\mathrm{d}l_{\mathrm{p}}}{\mathrm{d}t} = u_{\mathrm{p}} \tag{10}$$

The force balance of the inclusion is shown in Eq. (11).

$$\frac{\mathrm{d}u_{\mathrm{p}}}{\mathrm{d}t} = F_{\mathrm{D}} + \frac{(\rho_{\mathrm{p}} - \rho)g}{\rho_{\mathrm{p}}} + F_{i} \tag{11}$$

#### 2.1.3 Calculation removal rate

The removal rate of inclusion is calculated by the simulation results of the PBM model and DPM model. The removal rate  $P_i$  of the *i*th group and total removal rate P are shown in **Table 1:** Size parameters of swirling flow tundish model. Eqs. (12) and (13)

$$P_i = 1 - \frac{\left(N_{i, \text{out}} \times \left(1 - P_{d, i}\right)\right) \times V_i}{N_{i, \text{in}} \times V_i}$$
(12)

$$P = 1 - \frac{\sum_{i=1}^{i} (N_{i,\text{out}} \times (1 - P_{d,i})) \times V_{i}}{\sum_{i=1}^{i} N_{i,\text{in}} \times V_{i}}$$

$$(13)$$

In the formula,  $N_{i,out}$  and  $N_{i,in}$  are the quantity density of the *i*th group at the outlet and inlet of the tundish.  $P_{d,i}$  is the removal rate of the inclusion with a diameter of the ith group simulated by the DPM model, and  $V_i$  is the volume of one inclusion of the *i*th group.

## 2.2 The SFT model parameters

The schematic diagram of the SFT is shown in Figure 1, the SFT parameters are shown in Table 1. The NSCT parameters are the same as the SFT.

### 2.3 Boundary conditions

Sampling and testing of steel samples were conducted from the LF refining furnace in the factory. The test result shows that the size of inclusion was mainly the range of 1–120 µm, and the volume fraction of inclusion was 0.03%. It is assumed that the inclusions are evenly distributed in the molten steel in the initial state. The inclusions are divided into 16 groups according to the volume grouping method  $V_{i+1}/V_i = 2^{1/q}$  proposed by Lister, Smit, and Hounslow (1995). The volume ratio  $V_{i+1}/V_i$  = 2.6. Table 2 shows the parameters of each group. The density of inclusion is 3900 kg/m<sup>3</sup>.

For the PBM model, the velocity of molten steel is 1 m/s. The velocity of the inclusion at the inlet is the same as the molten steel. The tundish walls are non-slip boundaries, and the adhesion of inclusion by walls is ignored. The top

Parameter	Size/mm	Parameter	Size/mm
Bottom length	4500	Top length	5000
Bottom width	1250	Top width	1400
Diameter of SC	600	Height of SC	450
The inner diameter of the nozzle	100	Outlet diameter	75
The outer diameter of the nozzle	125	Dam height	625
Height	1250	Weirs depth	750

Table 2: Characteristic diameter, initial number density and volume fraction of each group of inclusion.

Groups	Characteristic diameter/µm	Initial number density/m <sup>-3</sup>	Volume fraction
1	1.00	$1.36\times10^{13}$	0.024
2	1.38	$1.83\times10^{13}$	0.083
3	1.89	$7.85\times10^{12}$	0.093
4	2.60	$2.81\times10^{12}$	0.086
5	3.58	$1.05\times10^{12}$	0.084
6	4.92	$\boldsymbol{5.59 \times 10^{11}}$	0.120
7	6.76	$\boldsymbol{2.38\times10^{11}}$	0.130
8	9.36	$6.50\times10^{10}$	0.093
9	12.80	$2.20\times10^{10}$	0.088
10	17.60	$3.29 \times 10^{9}$	0.030
11	24.20	$1.04\times10^9$	0.026
12	33.20	$5.11\times10^{8}$	0.033
13	45.80	$3.50\times10^8$	0.058
14	62.90	$6.93 \times 10^{7}$	0.030
15	86.50	$2.37 \times 10^{7}$	0.022
16	119.00	$5.13\times10^6$	0.015

surface is the free liquid surface. The outlet is set as the outflow boundary condition. The inclusions rebound when touching the wall. For the DPM model, the velocity of molten steel is 1 m/s. The velocity of the inclusion is the same as the molten steel at the inlet. The tundish walls are non-slip boundaries, the inclusions rebound when touching the wall. The inclusions are adsorbed when the inclusions move to the top layer.

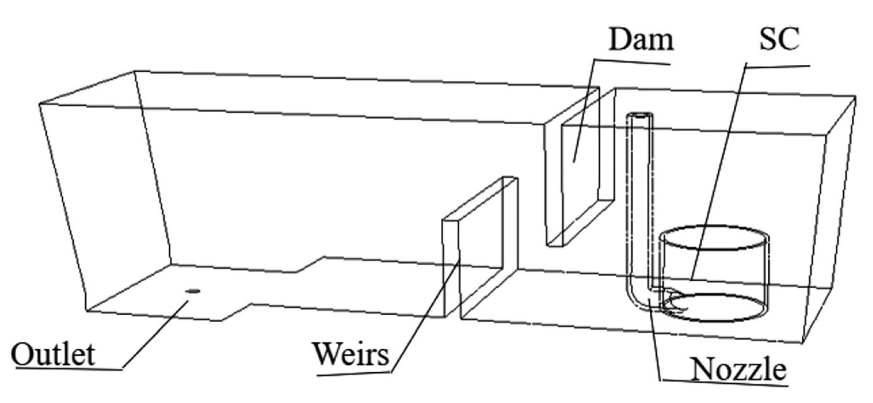


Figure 1: Schematic diagram of swirling flow tundish.

# 3 Results and discussion

## 3.1 Verify the flow state of the SFT

In the factory, it is difficult to detect the flow of molten steel in the tundish. Therefore the flow of molten steel in the numerical simulation was usually compared with the water model. As shown in Figures 2 and 3, the water model parameters are the same as the numerical simulation. It

shows that the flow state of the tracer between the water model and the numerical simulation agrees well.

#### 3.2 Collision-coalescence of inclusion

The behavior of inclusion movement is simulated with PBM model. The inclusions are treated as a continuous phase. The quantity density of inclusion at the outlet of the SFT

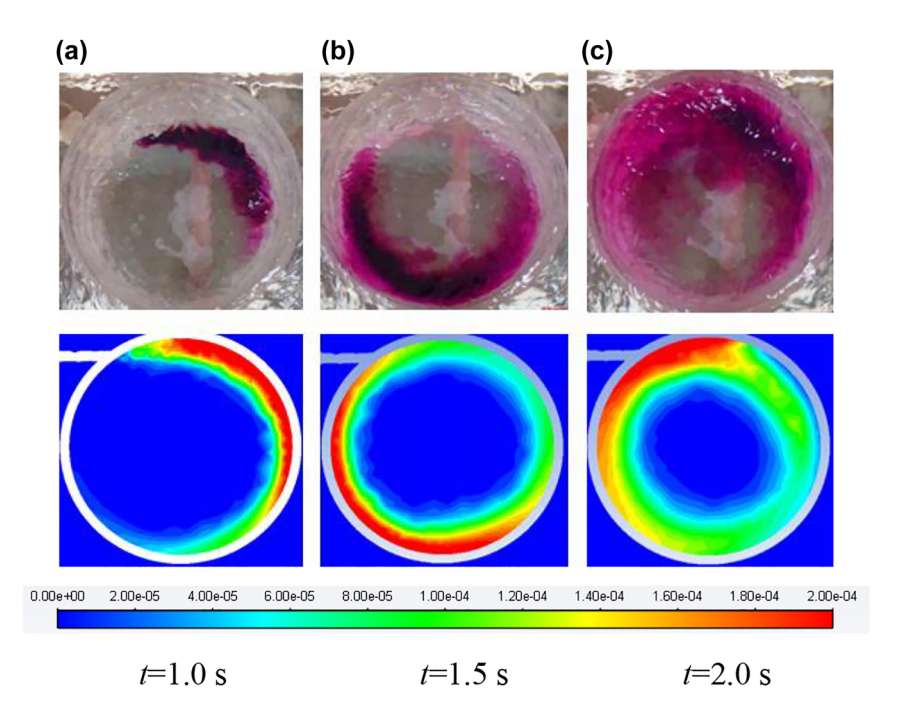


Figure 2: The flow of water model experiments and numerical simulation in SC.

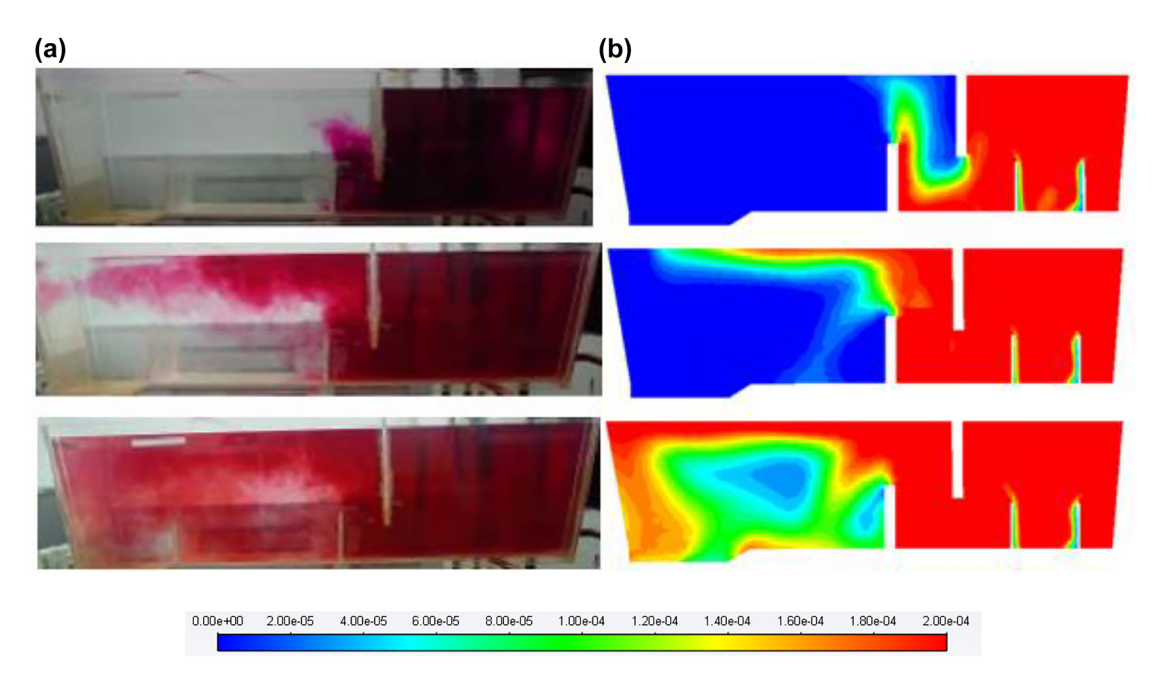


Figure 3: The flow of water model experiments and numerical simulation results in SFT.

Table 3: The quantity density of inclusion at the outlet.

Group	Feature diam- eter (µm)	NSCT number density	SFT number density	Difference ra- tio (%)
1	1.00	9.67E+12	9.12E+12	5.62
2	1.38	1.33E+13	1.26E+13	5.74
3	1.89	6.40E+12	6.08E+12	4.97
4	2.60	2.81E+12	2.40E+12	14.50
5	3.58	1.05E+12	9.19E+11	12.40
6	4.92	4.92E+11	4.73E+11	3.73
7	6.76	2.14E+11	2.07E+11	3.07
8	9.36	6.30E+10	6.18E+10	1.99
9	12.80	2.06E+10	2.18E+10	2.11
10	17.60	2.88E+09	2.74E+09	4.90
11	24.20	1.03E+09	9.38E+08	9.72
12	33.20	4.57E+08	4.40E+08	3.73
13	45.80	3.09E+08	2.95E+08	4.70
14	62.90	6.32E+07	5.99E+07	5.19
15	86.50	1.89E+07	1.80E+07	4.76
16	119.00	6.25E+06	7.31E+06	-16.82

and the NSCT is shown in Table 3. It is discovered that the quantity density of inclusion of groups 1-15 decreases, and the quantity density of inclusion of SFT is smaller than that of NSCT at the outlet.

Figure 4 shows the change of average diameter of inclusion in the tundish. The inclusions and molten steel enter tundish from the nozzle, the inclusions collide with each other and form larger-sized inclusions. The average diameter of inclusion increases gradually in SFT. With the introduction of SC, the turbulent kinetic energy of molten steel is mainly concentrated in the SC. The inclusions move towards the center of the SC because the density of inclusions is smaller than that of molten steel, which greatly increases the probability of collision between inclusions. The average diameter of the inclusion increases significantly in the zone above SC. The collision of inclusion is accompanied by the turbulent flow of molten steel. The small inclusions collide and coalesce into the larger ones.

Figure 5 shows the evolution of the average diameter at the outlet. The average diameter of NSCT increased from 3.93 µm to 4.25 µm, and the average diameter of inclusion increased by 8.14%. The average diameter of SFT increased from 3.93 µm to 4.35 µm, and the average diameter of inclusion increased by 10.68%. The average diameter of inclusion in the SFT is larger than the NSCT at the outlet. The turbulent kinetic energy of the molten steel is mainly concentrated in the SC, which promotes the rotation of molten steel in the SC. The inclusions move towards the center of SC because the density of inclusion is smaller than that of molten steel, which increases the probability of collision between inclusions and promotes collisioncoalescence.

Figure 6 shows the volume fraction of inclusion in tundish with and without considering collision. For the inclusions with sizes smaller than 25 µm, the volume fraction curve of inclusion with collision shifts to right, and the size of the inclusion increases. The volume fraction of small inclusion decreases, and the volume fraction of large inclusion increases. The inclusion volume fraction curve of the SFT with collision shifts to right compared with that of NSCT, which means that the inclusions in the SFT is more favorable to collide and aggregate than that in the NSCT.

#### 3.3 The removal rate of inclusion

The inclusions are removed due to floating to the top layer. Figure 7 is the removal rate without considering collision. The removal rate of inclusion increases with diameter. Most of the large-sized inclusions are removed by floating upwards, but the small-sized inclusions are difficult to float to the top layer. The removal rate of small-sized inclusion is low without considering collision.

Figure 8 shows the removal rate of inclusion with considering the collision-coalescence. The removal rate of inclusion with colliding is higher than that without colliding in the SFT. The total volume removal rate of inclusion increases from 30.09% to 43.20%. The swirl flow promotes inclusions to move towards the center of SC, which increases the collision probability of inclusion. The small inclusions collide and aggregate into large-size ones, the large inclusions are conducive to floating to the top layer. The removal rate of small inclusion increases more significantly than that of large inclusion. As the size of inclusion increases, the impact of collision frequency on the removal rate of inclusion gradually decreases. The small inclusions tend to aggregate when inclusions collide with each other, while large inclusions are hard to coalesce. There is a problem with collision efficiency. Higashitani et al. (Higashitani, Yamauchi, and Matsuno 1983) considered the interaction between fluid dynamics and inclusion particles, the effective cohesion coefficient of turbulence is proposed as:

$$\alpha = 0.732 \left(\frac{5}{N_{\rm T}}\right)^{0.242} \tag{15}$$

$$N_{\rm T} = \frac{6\pi\mu (d_i + d_j)^3}{8H} \cdot \sqrt{\frac{4\epsilon}{15\pi\nu}}$$
 (16)

 $N_{\rm T}$  is the ratio of viscous force to Vander Waals force, H is Hamaker constant.

The formulas show that the  $N_{\rm T}$  is proportional to the third power of the sum of the diameters of inclusions, and

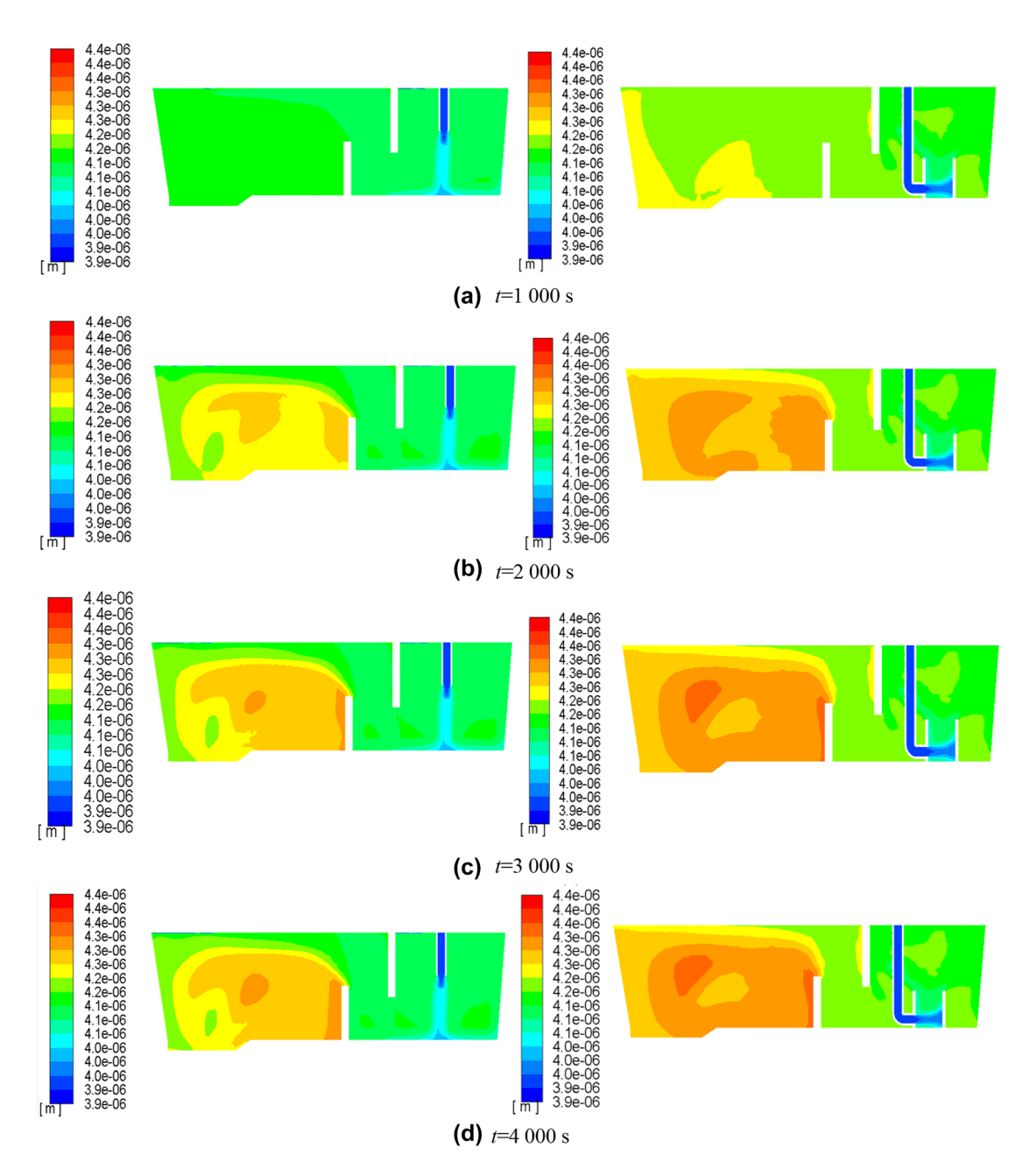
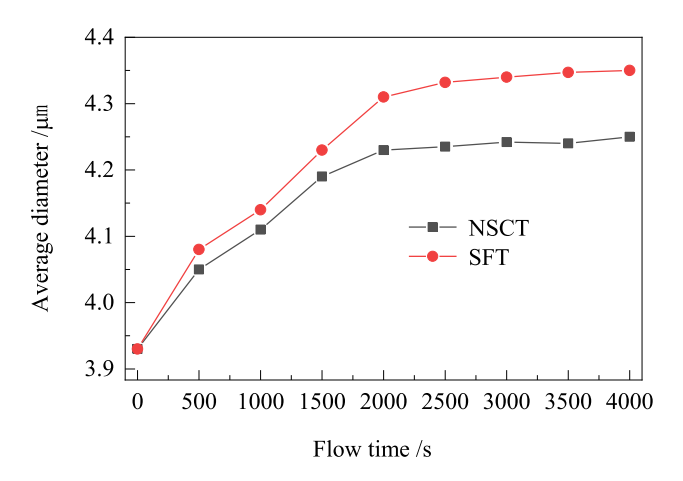


Figure 4: Change of average diameter of inclusion.

the effective cohesion coefficient decreases with the increase of  $N_{\rm T}$ . Therefore, the smaller the sum of the diameters of the inclusion, the easier it is to coalesce.

In Figure 8, the removal rate of inclusion increases with the increase of inclusion diameter for the SFT without colliding, which is not observed when the collision is considered. In this paper, the collision-coalescence and ignores the breakage of inclusion are considered with the help of PBM. The removal rate of inclusion consists of two parts. Firstly, the inclusions are removed by floating to the top layer. Secondly, the inclusions collide and aggregate

into larger-sized inclusions. For 1 µm inclusions, the inclusions collide and aggregate into larger inclusions, but no 1 µm inclusions are formed. Therefore, 1 µm inclusions have a higher removal rate. Similarly, for 119 µm size inclusions, no inclusions collide and aggregate into larger inclusions, and the smaller inclusions collide and aggregate into 119  $\mu m$  size inclusions. Therefore, the 119  $\mu m$  inclusions have a lower removal rate. At the inlet, 4.92 µm and 6.76 µm inclusions respectively account for 12% and 13% of the volume of all inclusion. The inclusions of 3.92  $\mu m$  and 6.76  $\mu m$  collide and aggregate into 9.36  $\mu m$ 



**Figure 5:** The average diameter of inclusion of SFT and NSCT with the flow time at the outlet.

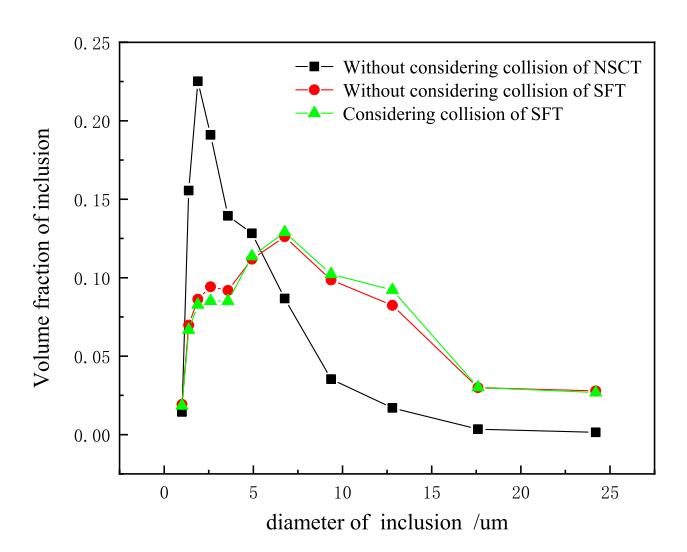


Figure 6: Volume fraction of inclusion.

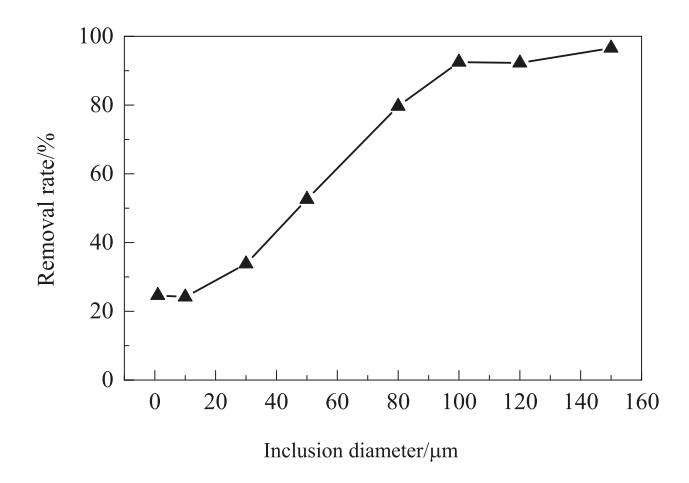


Figure 7: The removal rate of inclusion.

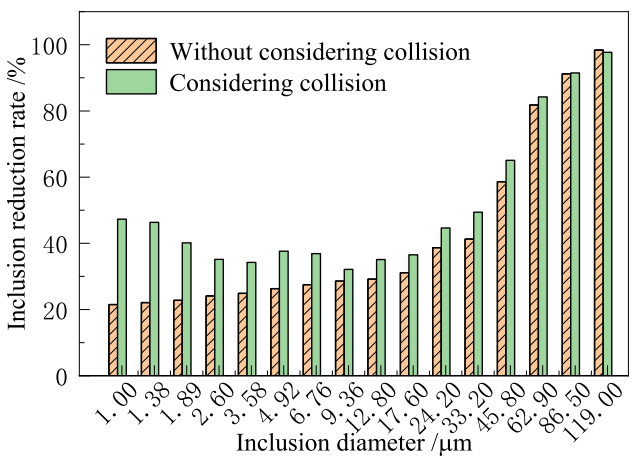


Figure 8: The removal rate of inclusion in SFT.

inclusions, which leads to a low removal rate of 9.36  $\mu$ m. Therefore, the removal rate of inclusions does not increase with the increase of inclusion diameter.

## 4 Conclusions

In the tundish, the inclusions collide and aggregate along with the flow of liquid steel. In this paper, the effect of the SC on the collision-coalescence of inclusion was investigated. The introduction of the SC promotes the collision-coalescence of inclusion. The effect of collision-coalescence on the removal rate of inclusion was investigated. It was found that collision-coalescence increased the removal of small inclusion and increased the total volume removal rate of inclusion.

- (1) The introduction of the SC promotes the collision-coalescence of inclusion. The average diameter of NSCT increased from 3.93 μm to 4.25 μm with increasing by 8.14%. The average diameter of SFT increased from 3.93 μm to 4.35 μm with increasing by 10.68%.
- (2) The collision-coalescence improved the removal rate of inclusion. With considering the collision-coalescence of inclusion, the removal rate in the SFT increased from 30.09% to 43.20%. The removal rate of small inclusion increased more significantly.

**Author contributions:** All the authors have accepted responsibility for the entire content of this submitted manuscript and approved submission.

**Research funding:** This work was supported by the National Natural Science Foundation of China (grant number 51604068).

Conflict of interest statement: The authors declare no conflicts of interest regarding this article.

## References

- Abrahamson, J. 1975. "Collision Rates of Small Particles in a Vigorously Turbulent Fluid." Chemical Engineering Science 30: 1371.
- Chen, D., X. Xie, and M. Long. 2014. "Hydraulics and Mathematics Simulation on the Weir and Gas Curtain in Tundish of Ultrathick Slab Continuous Casting." Metalurgical and Materials Transactions B 45 (2): 392-398.
- Hou, Q. F., Q. Yue, and H. Y. Wang. 2008. "Modelling of Inclusion Motion and Flow Patterns in Swirling Flow Tundish with Symmetrical and Asymmetrical Structure." ISIJ International 48: 787.
- Hou, Q. F., and Z. S. Zou. 2005. "Comparison Between Standard and Renormalization Group k-e Models in Numerical Simulation of Swirling Flow Tundish." ISIJ International 45: 325.
- Higashitani, K., K. Yamauchi, and Y. Matsuno. 1983. "Turbulent Coagulation of Particles Dispersed in a Viscous Fluid." Journal of Chemical Engineering of Japan 16: 299.
- Kusters, K. A., J. G. Wijers, and D. Thoenes. 1997. "Aggregation Kinetics of Small Particles in Agitated Vessels." Chemical Engineering Science 52: 107.
- Lister, J. D., D. J. Smit, and M. J. Hounslow. 1995. "Adjustable Discretized Population Balance for Growth and Aggregation." AIChE Journal 41: 591.

- López-Ramirez, S., J. Palafox-Ramos, R. D. Morales, J. de J. Barreto, and D. Zacharias. 2001. "Modeling Study of the Influence of Turbulence Inhibitors on the Molten Steel Flow, Tracer Dispersion, and Inclusion Trajectories in Tundishes." Metallurgical and Materials Transactions B 32 (4): 615-27.
- Morales, R. D., D. Cruz, P. Ramos, L. Ramirez, and D. J. B. Sandoval. 2001. "Modelling Steel Flow in a Three-Strand Billet Tundish Using a Turbulence Inhibitor." Steel Reseach 72 (1): 11-16.
- Saffman, P. G., and J. S. Turner. 1956. "On the Collision of Drops in Turbulent Clouds." Journal of Fluid Mechanics 1: 16.
- Wang, Q. Q., L. F. Zhang, and S. Seetharaman. 2016. "Detection of Non-Metallic Inclusions in Centrifugal Continuous Casting Steel Billets." *Metallurgical and Materials Transactions B* 47: 1594.
- Wang, F., B. K. Li, and F. Tsukihashi. 2007. "Large Eddy Simulation on Flow Structure in Centrifugal Flow Tundish." ISIJ International 47:
- Yue, Q., Q. F. Hou, and Z. S. Zou. 2009. "Numerical Simulation of Flow Field in a Swirling Flow Tundish." Metallic Materials 8: 81.
- Yue, Q., Q. F. Hou, and Z. S. Zou. 2010. "Aggregation Kinetics of Inclusions in Swirling Flow Tundish for Continuous Casting." Journal of Iron and Steel Research 17: 6.
- Yue, Q., Q. F. Hou, and Z. S. Zou. 2009. "Water Modeling of Swirling Flow Tundish for Steel Continuous Casting." Journal of Iron and Steel Research 16: 17.
- Yang, B., H. Lei, and Q. Bi. 2018. "Numerical Simulation of Collision-Coalescence and Removal of Inclusions in a Tundish." Journal of Occupational Medicine 70: 2950.